Documentation EML-Evaluation-Software and Discussion of the Results from Parabolic-Flight-Experiments PF2014B

Stephan Rietzler

18. Juni 2015

Inhaltsverzeichnis

Zusammenfassung

This document summarizes the results of the project-work to evaluate the electromagnetic-levitation-experiments conducted in october 2014 to determine the surface-tension and viscosity of four alloys as a function of temperature (in the vincity of the melting temperature of the alloys). It gives a short overview of the experimental setup and the software that is used. The main focus is on the derived results. It also highlights some open questions and possible improvements.

1 Experimental Setup and Data-Evaluation

From each of the investigated alloys one sample (sphere with radius of approx. $3mm$ and mass of $1g$) was prepared in Ulm. This one sample of each alloy was processed in several (not necessarily consecutive) parabola-flights. That means it was heated above melt-temperature [1] and than cooled. Heating of the samples was achieved by inducing currents in the sample [2]. On some experimental runs there were additional heat-pulses (i.e. electromagnetic pulses) in the cooling-phase to stimulate oscillation of the sphere. Cooling was achieved by floating the experimental chamber with gas. Cooling rates of approx. $50 - 100\frac{K}{s}$ where achieved and necessary, as the time was limited to approx $20s$ of zero-G during one parabolic flight. The question arises as this convective cooling is consitent with the assumptions of free oscillation of the sphere. During the experiment the sample was filmed by two optical cameras (frame-rate of 200Hz for radial-view and 150Hz for axial-view) and a pyrometer which recorded temperature. I assume that there is only one radial-view-camera as the experimental setup implies axial symmetry. As shown in the results section this is measurably not the case, although the effects are small. Additional parameters like e.g. pressure, accelaration ... where also recorded.

The following facts have to be kept in mind:

- To measure the temperature of the alloy the pyrometer needs to be calibrated with the emissivity of the alloy-surface. In general this emissivity is temperature dependent. As this dependence is unknow, the pyrometer is calibrated with a constant emissivity (measured at a certain phase-transition of the alloy). Therefore the measured Temperature has to be corrected (in the best case only) with a offset. **This temperature-offset-correction is not done in the presented results.**
- To convert the determined damping constant τ of the oscillation to a viscosity ($\eta = \frac{3}{10\pi}\frac{m}{r}\cdot\tau^{-1}$) one needs the radius of the sample! The viscosity in this work is calculated with the radius of the sample-sphere at room-temperature.
- To determine the damping constant one needs to analyse the signal over at least one second. As the sample cools with cooling rates of appox.

[1] How much above T_{melt}? reasons?
[2] Differences/Influences of heating- and positioning-fields?

$50 - 100\frac{K}{s}$ the assignment of viscosity to temperature is in the best case a rough approximation.

- To determine the frequency of the sphere-oscillation one also needs to analyse the signal for a certain time-span. The default time-span used in this evaluation is $1s$. To assign a frequency (surface-tension $\sigma = \frac{3}{8}\pi M\nu^2$) to a time (temperature) I have used the midpoint of the timewindow.

2 Software

In this project three software packages are used:

1. Tevi-Software: Supplies edge-detection algorithms with which the oscillation of the edges of the projected sample-surface can be detected. Having the edges detected, the center of mass (two degress of freedom) and ellipsoids (three degrees of freedom, i.e. two radii and orientation) are fitted to the edges. Implementation of these algorithms is in proprietary software and can not be checked. Result of the data-processing with this software is a dataset (one for each camera) with the relevant variables, especially center of mass coordinates, radii of two ellipsoids (orientation is manually set so that they are rotated 45° relativ to each other; this assures that the additional information is maximally independend), temp of samples ....

2. Matlab: Graphical user-interface to visualize the signals (radii, temp ...), calculate and visualize the Fourieranalysis of the signals and produce datasets (surface-tension vs. temp and viscosity vs. temp) for each alloy.

Possible Improvements: Implement all data-processing steps in phyton. Thus the software would be maintainable, improvable and comprehensible. Up to date software like OpenCV for edge-detection could be easily included.

2.1 EML-Evaluation-GUI; Documentation

2.1.1 Datenaufbereitung

Mit Hilfe der Tevi-Software wird aus den Kamera-Aufnahmen ein ASCII-File erzeugt das unter anderem folgende für die weitere Auswertung wichtige Daten enthält: Bz (Beschleunigung), Temp und 2 Radien-Paare. Die zugehörigen Ellipsen sind immer 45° gegeneinander gedreht, so dass man maximale Unabhängigkeit erreicht. Dieser Datensatz wird nun mit der von mir geschriebenen Software automatisch ausgewertet um die relevanten Größen Oberflächenspannung und Viskosität als Funktion der Temperatur zu erhalten. Die prinzipielle Logik werde ich im folgenden erläutern. (Bem.: Alle erwähnten Parameter sind änderbar, ich gebe jeweils die Default-Werte an.)

Aus einem Parabelflug erhält man zwei Datensätze mit jeweils 8 relvanten Signalen: Die beiden Radien-Paare sowie Summe und Differenz dieser Paare. Zusätzlich erzeuge ich einen weiteren Datensatz, indem ich die beiden Datensätze kombiniere. Hierzu interpoliere ich die Daten der Axial-Kamera auf

200Hz und führe diesen Datensatz dann mit dem Radial-Kamera-Datensatz zusammen. Synchronisiert werden die Datensätze anhand der absoluten Zeit. Dieser Datensatz enthält dann alle 16 relevanten Signale.

Nun wird für jeden Datensatz jedes Signal folgendermassen ausgewertet:

1. Zeitaufgelöste FFT, d.h. ein Zeitfenster (default 1s) wird in 0.1s Schritten über das Signal "geschoben". Pro Zeitfenster ermittle ich folgende Größen aus dem Periodogramm: Dominante Frequenz und Periodogramm-Ordinate dieser Frequenz als Maß für die "Amplitude" der dominanten Frequenz. (Bemerkung: Die Periodogramm-Ordinate kann nur als Masszahl zum Vergleich von "Amplituden" aus unterschiedlichen Zeitfenstern verwendet werden falls die Zeitfenster gleich lang sind und die Samplerate sich nicht ändert!)

2. Die beiden so ermittelten Werte werden dem Zeitfenster-Mittelpunkt zugeordnet.

3. Eine Zuordnung von Zeit zu Temperatur bekomme ich indem ich für die Zeit zwischen maximaler Temperatur und Wiedererstarrung der Probe eine Gerade anpasse.

4. Damit habe ich dann folgende Zuordnung:

   $$Zeit \leftrightarrow Temp \rightarrow (dominante\, Frequenz, Amplitude\, der\, dominanten\, Frequenz)$$

5. Aus der ermittelten Frequenz ermittle ich dann mit der Formel $\sigma = \frac{3}{8} \cdot \pi \cdot M \cdot \nu^2$ die Oberflächenspannung und erhalte daraus die Zuordnung:

   $$Temp \rightarrow \sigma$$

   .

6. Die Viskosität η berechnet sich aus Dämpfungszeitkonstanten τ mit der die Amplitude der dominanten Frequenz abnimmt: $\eta = \frac{3}{20\pi} \frac{M}{R} \tau^{-1}$. Die Dämpfung habe ich ermittelt indem ich eine exp-Funktion an die Periodogramm-Ordinaten (Maß für die Amplitude) gefittet habe. Da die Datenqualität sehr schlecht ist muss die Dämpfung über einen möglichst langen Zeitraum ermittelt werden um die Varianz der Dämpfungsschätzung in einen vertretbaren Maß zu halten. Ich habe mich entschieden, jeweils den maximal möglichen Zeitraum zu nutzen in dem die Probe "frei" schwingt. D.h. den Zeitraum zwischen jeweils zwei Experiment-Ereignissen wie z.B. Ende Heizphase bis erster Heizpuls, Zeitraum zwischen zwei Heizpulsen .... Dies bedingt zwei gewichtige Nachteile: Pro Signal gibt es nur 1 + (Anzahl Heizpulse) Viskositäts-Werte. Zum zweiten ist die Zeitauflösung der Viskositätswerte sehr schlecht. Der Viskositätswert bzw. die Dämpfungskonstante wird wieder dem Zeitmittelpunkt des Zeitfensters zugeordnet. Die entgültige Zuordnung der Viskosität zu einer Temperatur wird noch problematischer wenn man berücksichtigt das die Proben mit einer Rate von ca. 50-100 K/s abkühlen. Bei einem mittleren Zeitfenster von ca. 2 s wird damit eine Probentemperatur von 100-200K überstrichen.

7. Zusammenfassend erhält man damit für jedes Signal Daten entsprechend folgender Zuordnung:

$$Temp \rightarrow \sigma$$

$$Temp \rightarrow \eta$$

Da die Probe im Schnitt 4-5 s frei schwingt erhält man typischerweise 40-50 Datenpaare (Temp,Oberflächenspannung) pro Signal. Viskositätswerte erhält man je nach Anzahl der Heizpulse, aber maximal 3 werte pro signal.

8. Die für jedes Signal erhaltenen Zuordnungen $Temp \rightarrow \sigma$ und $Temp \rightarrow \eta$ werden nun pro Parabelflug zusammengefasst. D.h. es kann durchaus vorkommen das zu einem Temperaturwert mehrere Viskositäts- und Oberflächenspannungen vorliegen. Diese sind allerdings nicht als unabhängige Messungen zu interpretieren, sondern im Gegenteil mehr oder weniger stark abhängig da sie z.T. nur aus einer Transformation der primären Signale (d.h. sind die vier Radien, die selbst schon nicht voneinander unabhängig sind) ermittelt wurden. Als Ergebnis für den Zusammenhang Temp/Viskosität bzw. Temp/Oberflächenspannung wurde eine Gerade an diese Werte gefittet.

9. Die Ergebnisse kann man sich interaktiv von der Software darstellen lassen. Man wird feststellen das sich die Ergebnisse von Datensatz zu Datensatz und von Parabelflug zu Parabelflug zum Teil signifikant unterscheiden.

10. Als Endergebniss für die jeweilige Metalllegierung habe ich den Mittelwert der Ergebnisse der auswertbaren Parabelflüge angegeben.

3 Results

3.1 Remarks

3.1.1 Experimental Setup

Pyrometer seems inert!

- Melting-Temp as measured by Pyrometer is always smaller than nominal Melt-Temp (determined with DSC).
- Temp-Measurement continues linearly after end of zero-G-Phase. Compare CuNiSi Pb11.
- Temp. of sample increases after heating is switched of.

3.1.2 Modes; Identification, Transition ...

Sauerland [DisSa93] claims that:

- If there is no rotational symmetry there is no degeneration of oscillatory modes. In principle modes might be distinguished, as certain combinations of measured signals are more sensitive to certain modes. In practice, this seems of no avail. A more pracmatic approch to detect oscillatory modes would be to generate a database of simulations and train a statistical learner on this database.
- Frequency-splitting of modes belonging to the same angular momentum main-mode l is to small to be detactable with the achieved frequency-resolution of approx. $1Hz$.
- Sauerland claims (and shows for m=0 modes, which have axial symmetry) that l=1 modes are not influenced by surface tension. This seems strange, as obviously these modes (besides moving the center of mass) deform the sphere-surface! See (see Figure (1)). Remark: In deducing the Rayleigh-Formula $\omega_l^2 = l(l+2)(l-1)\frac{\sigma}{\rho \cdot a^3}$ he assumes a rotation- and divergence-free velocity-field v! ($v = \nabla\phi, \nabla \cdot v = \Delta\phi = 0$). Then he chooses the following Ansatz for $\phi = \sum_{l=0}^{\infty} \beta_l r^l P_l(\mu)$. This is not the most general solution for $\Delta\phi = 0$, even for axial-symmetrical problems! So what is the justification for this Ansatz? A nice (but doubtful, esp. for l=1) solution?
- **Oscillatory modes of higher order:** In chapter 10.2 Sauerland gives formulas for oscillation-frequencies of modes higer than l=2. If $\omega_{l=2}$ is the frequency of mode l=2, than the next frequencies are given as: $\omega_{l=3} = 1.92 \cdot \omega_{l=2}$; $\omega_{l=4} = 3 \cdot \omega_{l=2}$. Very often you can see another peak in the periodogramm at approx. twice the dominant frequency. According to the given formulas this peak could be caused by l=3 mode oscillations or by higher order harmonics.

Spherical Harmonics

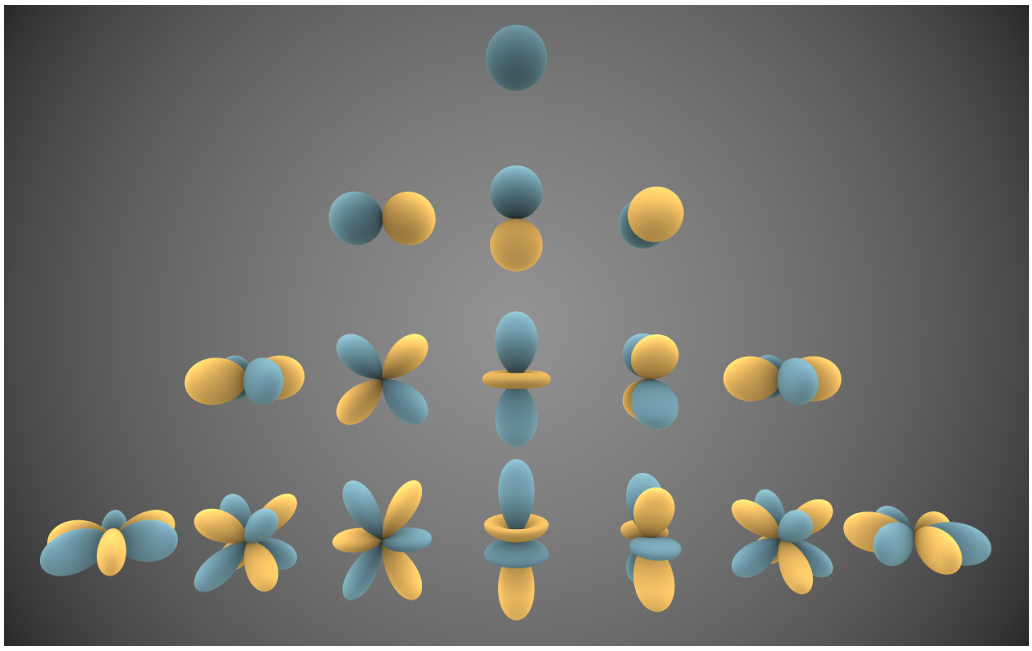

Abbildung 1: Visual representations of the first few real spherical harmonics. Blue portions represent regions where the function is positive, and yellow portions represent where it is negative. The distance of the surface from the origin indicates the value of $Y_l^m(\theta, \phi)$ in angular direction (θ, ϕ).

Symmetry-Considerations Representative for all experimental runs I have depicted the movement of the sample CuNiSi Pb15 in the levitation-field as represented by the centerpoint-coordinates (see Figure (2)). Clearly you can see that the radial- and axial-symmetry is broken. Therefore it has to be expected that the $2l+1$ modes belonging to the same l are no longer degenerate. But due to the limited frequency-resolution this broken symmetry may not be detected.

Another point to notice here is: Although the frequencies with wich the sample oscillates in the levitation-field differs from alloy to alloy, these frequencies are all in the range of $2-5Hz$. This oscillation can cause a modulation of the measured radii (movement to and from camera increases/decrases the measured radii, compare [DisSa93]).

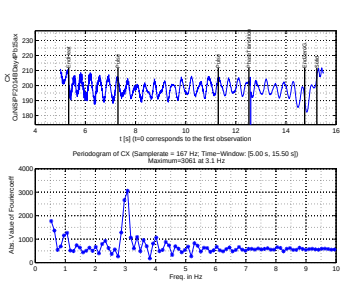

(a) Pb15ax-CX

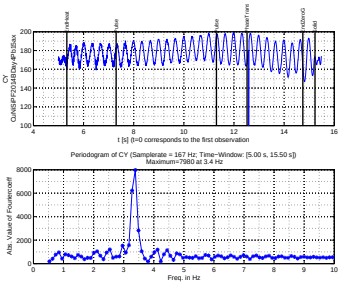

(b) Pb15ax-CY

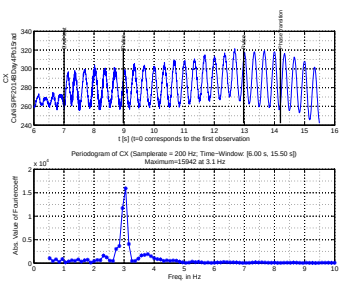

(c) Pb15rad-CX

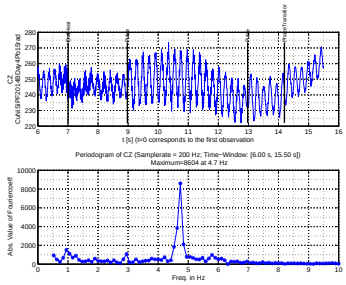

(d) Pb15rad-CZ

Abbildung 2: CuNiSi; Pb15; Centerpoint-Coordinates in Pixel with Periodogramm; CX is measured twice: Once from the radial-cam and once from the axial cam;

3.1.3 Surface-Tension

Surface-tension of the alloy is calculated with the Rayleigh-Formula

$$\sigma = \frac{3\pi}{8} M\omega^2.$$

To estimate the time-resolved frequency (surface-tension) of the signal I have used $1s$ time-windows. The frequency-resolution is accordingly $1Hz$. (The software allows to adjust this windowsize and therefore the frequency-resolution.) These windows are shifted by $.1s$ timesteps through the timerange of the experiment. Inherent in this procedure is the fact that the frequencies are highly correlated as the timewindows overlap. These two facts cause the signal (frequency/surface-tension vs time) to look like a step-function.

Each parabola-flight gives one dataset for each camera from which eight signals are extracted:

For radial-cam: RX, RY, diffRXY, sumRXY, RXrot, RYrot, diffRXYrot, sumRYrot.

For axial-cam: RX, RZ, diffRXZ, sumRXZ, RXrot, RZrot, diffRXZrot, sumRXZrot.

The appendix rot indicates a coordinate system which is turned 45° to the first one. Obviously these 8/16 signals for one experimental run are not independent!

The question arises, which one to use if they yield different results? Certainly this is one point that needs to be claryfied. In this report I show that they do indeed yield significant different results.

3.1.4 Viscosity

To calculate the viscosity one needs to estimate damping-constants from the signals. The estimated damping-constant is highly dependent on the timespan used. Another point is: The shorter the timespan, the higher the variability of the estimated damping-constant. To keep this variability and subjective choices as low as possible I have used the maximum timespans between end of heating - heatpulse 1 - (heatpulse 2) - end of zero G phase/ resolidification. This procedure gives two (three) damping-constants for each signal. The so determined damping-constant is associated to the midpoint of the time- (temp-) intervall used. The time/temp resolution of the viscosity is therfore very low.

3.2 Cu-Ni-Si-Alloy

3.2.1 Comments on Datasets

Pb 11

- Temp-Diagramm looks peculiar. Sudden Temperature drop at the end of cooling phase!
- Temprature of Sample seems to rise slightly after end of heating!

Pb 13

- Temp-Diagramm looks peculiar. Sudden Temperature drop at the end of cooling phase!
- Temprature of Sample seems to rise slightly after end of heating!

Pb 14

- Temp-Diagramm looks peculiar. Sudden Temperature drop at the end of cooling phase!
- Temprature of Sample seems to rise slightly after end of heating!

3.2.2 Results

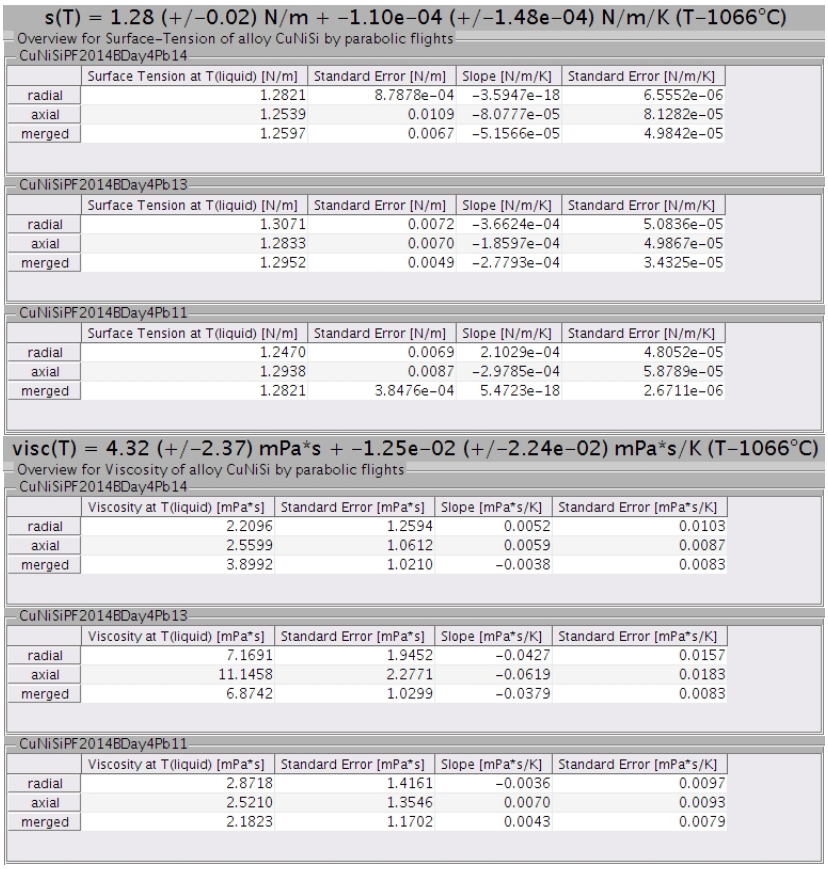

s(T) = 1.28 (+/-0.02) N/m + -1.10e-04 (+/-1.48e-04) N/m/K (T-1066°C)

Overview for Surface-Tension of alloy CuNiSi by parabolic flights

CuNiSiPF2014BDay4Pb14

	Surface Tension at T(liquid) [N/m]	Standard Error [N/m]	Slope [N/m/K]	Standard Error [N/m/K]
radial	1.2821	8.7878e-04	-3.5947e-18	6.5552e-06
axial	1.2539	0.0109	-8.0777e-05	8.1282e-05
merged	1.2597	0.0067	-5.1566e-05	4.9842e-05

CuNiSiPF2014BDay4Pb13

	Surface Tension at T(liquid) [N/m]	Standard Error [N/m]	Slope [N/m/K]	Standard Error [N/m/K]
radial	1.3071	0.0072	-3.6624e-04	5.0836e-05
axial	1.2833	0.0070	-1.8597e-04	4.9867e-05
merged	1.2952	0.0049	-2.7793e-04	3.4325e-05

CuNiSiPF2014BDay4Pb11

	Surface Tension at T(liquid) [N/m]	Standard Error [N/m]	Slope [N/m/K]	Standard Error [N/m/K]
radial	1.2470	0.0069	2.1029e-04	4.8052e-05
axial	1.2938	0.0087	-2.9785e-04	5.8789e-05
merged	1.2821	3.8476e-04	5.4723e-18	2.6711e-06

visc(T) = 4.32 (+/-2.37) mPa*s + -1.25e-02 (+/-2.24e-02) mPa*s/K (T-1066°C)

Overview for Viscosity of alloy CuNiSi by parabolic flights

CuNiSiPF2014BDay4Pb14

	Viscosity at T(liquid) [mPa*s]	Standard Error [mPa*s]	Slope [mPa*s/K]	Standard Error [mPa*s/K]
radial	2.2096	1.2594	0.0052	0.0103
axial	2.5599	1.0612	0.0059	0.0087
merged	3.8992	1.0210	-0.0038	0.0083

CuNiSiPF2014BDay4Pb13

	Viscosity at T(liquid) [mPa*s]	Standard Error [mPa*s]	Slope [mPa*s/K]	Standard Error [mPa*s/K]
radial	7.1691	1.9452	-0.0427	0.0157
axial	11.1458	2.2771	-0.0619	0.0183
merged	6.8742	1.0299	-0.0379	0.0083

CuNiSiPF2014BDay4Pb11

	Viscosity at T(liquid) [mPa*s]	Standard Error [mPa*s]	Slope [mPa*s/K]	Standard Error [mPa*s/K]
radial	2.8718	1.4161	-0.0036	0.0097
axial	2.5210	1.3546	0.0070	0.0093
merged	2.1823	1.1702	0.0043	0.0079

Abbildung 3: Zusammenfassung der Ergebnisse für die CuNiSi-Legierung.

3.3 g-Ti-Al-Ta-Alloy

3.3.1 Comments on Datasets

Pb 26

Pb 27 Dataset is not analysable (see Figure (4)).

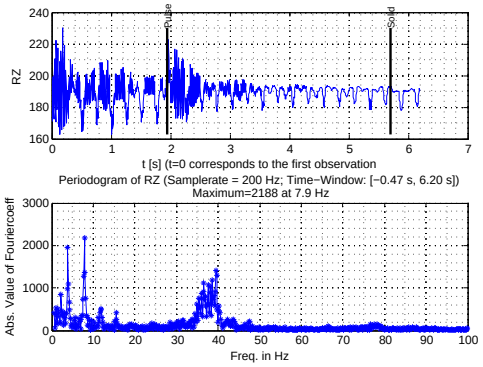

Abbildung 4: γ-TiAlTa from Parabola-Flight 27; Signal from radius RZ shows data-quality. Other signal have similar quality.

Pb 28

Pb 29

Pb 30

3.3.2 Results

s(T) = 1.24 (+/−0.07) N/m + −1.77e−04 (+/−3.14e−04) N/m/K (T−1614°C)

Overview for Surface−Tension of alloy gTiAlTa by parabolic flights

gTiAlTaPF2014BPb30

	Surface Tension at T(liquid) [N/m]	Standard Error [N/m]	Slope [N/m/K]	Standard Error [N/m/K]
radial	1.2769	0.0045	1.5526e−04	2.6898e−05
axial	1.2615	4.1422e−04	0	2.4359e−06
merged	1.2697	0.0029	8.0546e−05	1.7318e−05

gTiAlTaPF2014BPb29

	Surface Tension at T(liquid) [N/m]	Standard Error [N/m]	Slope [N/m/K]	Standard Error [N/m/K]
radial	1.0976	0.0047	−8.6114e−04	3.1350e−05
axial	1.1372	0.0075	−5.1197e−04	5.1604e−05
merged	1.1154	0.0046	−7.1146e−04	3.1114e−05

gTiAlTaPF2014BPb28

	Surface Tension at T(liquid) [N/m]	Standard Error [N/m]	Slope [N/m/K]	Standard Error [N/m/K]
radial	1.2618	0.0048	−7.1092e−05	3.1825e−05
axial	1.2544	0.0052	−1.2593e−04	3.4110e−05
merged	1.2556	0.0035	−1.0645e−04	2.3239e−05

gTiAlTaPF2014BPb27

	Surface Tension at T(liquid) [N/m]	Standard Error [N/m]	Slope [N/m/K]	Standard Error [N/m/K]
radial	1.2835	0.0068	−4.2439e−05	3.8467e−05
axial	1.2863	0.0060	1.6274e−05	3.4852e−05
merged	1.2895	0.0042	1.8662e−05	2.3944e−05

gTiAlTaPF2014BPb26

	Surface Tension at T(liquid) [N/m]	Standard Error [N/m]	Slope [N/m/K]	Standard Error [N/m/K]
radial	1.2632	0.0046	−1.5854e−04	2.8172e−05
axial	1.2654	0.0045	−1.8332e−04	2.8198e−05
merged	1.2646	0.0033	−1.6408e−04	2.0373e−05

visc(T) = 7.62 (+/−0.54) mPa*s + −3.01e−02 (+/−8.08e−03) mPa*s/K (T−1614°C)

Overview for Viscosity of alloy gTiAlTa by parabolic flights

gTiAlTaPF2014BPb30

	Viscosity at T(liquid) [mPa*s]	Standard Error [mPa*s]	Slope [mPa*s/K]	Standard Error [mPa*s/K]
radial	6.8503	0.8346	−0.0426	0.0052
axial	7.5845	1.3344	−0.0328	0.0083
merged	7.2952	0.6629	−0.0401	0.0041

gTiAlTaPF2014BPb29

	Viscosity at T(liquid) [mPa*s]	Standard Error [mPa*s]	Slope [mPa*s/K]	Standard Error [mPa*s/K]
radial	7.7097	0.5408	−0.0440	0.0039
axial	8.0066	1.3386	−0.0184	0.0097
merged	8.0789	0.5673	−0.0369	0.0041

gTiAlTaPF2014BPb28

	Viscosity at T(liquid) [mPa*s]	Standard Error [mPa*s]	Slope [mPa*s/K]	Standard Error [mPa*s/K]
radial	6.0843	0.5991	−0.0324	0.0031
axial	8.1683	1.1102	−0.0144	0.0058
merged	6.9729	0.5896	−0.0260	0.0031

gTiAlTaPF2014BPb27

	Viscosity at T(liquid) [mPa*s]	Standard Error [mPa*s]	Slope [mPa*s/K]	Standard Error [mPa*s/K]
radial	7.7294	0.7311	−0.0235	0.0054
axial	7.4932	0.7325	−0.0198	0.0053
merged	7.4741	0.5405	−0.0208	0.0040

gTiAlTaPF2014BPb26

	Viscosity at T(liquid) [mPa*s]	Standard Error [mPa*s]	Slope [mPa*s/K]	Standard Error [mPa*s/K]
radial	9.2971	0.7311	−0.0224	0.0046
axial	6.7661	0.6247	−0.0325	0.0039
merged	8.2759	0.5362	−0.0265	0.0034

Abbildung 5: Zusammenfassung der Ergebnisse für die $\gamma - TiAlTa$-Legierung.

3.4 Zr with 3% (at) Oxygen

3.4.1 Comments on Datasets

Pb 14

- Sample supercools to approx 1625 °C. Temperature-Curve shows not abnormalities.

Pb 15

- Sample supercools to approx 1625 °C. Temperature-Curve shows not abnormalities.

Pb 30

- Sample supercools to approx 1625 °C. Temperature-Curve shows not abnormalities.

3.4.2 Results

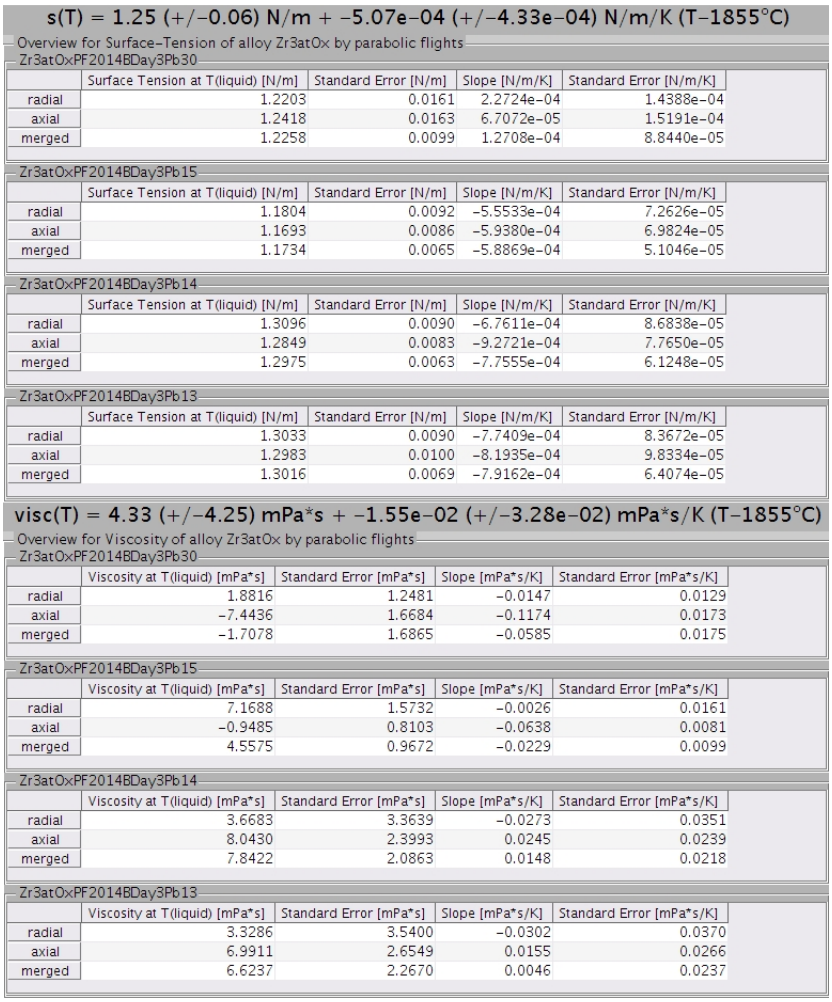

s(T) = 1.25 (+/−0.06) N/m + −5.07e−04 (+/−4.33e−04) N/m/K (T−1855°C)

Overview for Surface-Tension of alloy Zr3atOx by parabolic flights

Zr3atOxPF2014BDay3Pb30

	Surface Tension at T(liquid) [N/m]	Standard Error [N/m]	Slope [N/m/K]	Standard Error [N/m/K]
radial	1.2203	0.0161	2.2724e−04	1.4388e−04
axial	1.2418	0.0163	6.7072e−05	1.5191e−04
merged	1.2258	0.0099	1.2708e−04	8.8440e−05

Zr3atOxPF2014BDay3Pb15

	Surface Tension at T(liquid) [N/m]	Standard Error [N/m]	Slope [N/m/K]	Standard Error [N/m/K]
radial	1.1804	0.0092	−5.5533e−04	7.2626e−05
axial	1.1693	0.0086	−5.9380e−04	6.9824e−05
merged	1.1734	0.0065	−5.8869e−04	5.1046e−05

Zr3atOxPF2014BDay3Pb14

	Surface Tension at T(liquid) [N/m]	Standard Error [N/m]	Slope [N/m/K]	Standard Error [N/m/K]
radial	1.3096	0.0090	−6.7611e−04	8.6838e−05
axial	1.2849	0.0083	−9.2721e−04	7.7650e−05
merged	1.2975	0.0063	−7.7555e−04	6.1248e−05

Zr3atOxPF2014BDay3Pb13

	Surface Tension at T(liquid) [N/m]	Standard Error [N/m]	Slope [N/m/K]	Standard Error [N/m/K]
radial	1.3033	0.0090	−7.7409e−04	8.3672e−05
axial	1.2983	0.0100	−8.1935e−04	9.8334e−05
merged	1.3016	0.0069	−7.9162e−04	6.4074e−05

visc(T) = 4.33 (+/−4.25) mPa*s + −1.55e−02 (+/−3.28e−02) mPa*s/K (T−1855°C)

Overview for Viscosity of alloy Zr3atOx by parabolic flights

Zr3atOxPF2014BDay3Pb30

	Viscosity at T(liquid) [mPa*s]	Standard Error [mPa*s]	Slope [mPa*s/K]	Standard Error [mPa*s/K]
radial	1.8816	1.2481	−0.0147	0.0129
axial	−7.4436	1.6684	−0.1174	0.0173
merged	−1.7078	1.6865	−0.0585	0.0175

Zr3atOxPF2014BDay3Pb15

	Viscosity at T(liquid) [mPa*s]	Standard Error [mPa*s]	Slope [mPa*s/K]	Standard Error [mPa*s/K]
radial	7.1688	1.5732	−0.0026	0.0161
axial	−0.9485	0.8103	−0.0638	0.0081
merged	4.5575	0.9672	−0.0229	0.0099

Zr3atOxPF2014BDay3Pb14

	Viscosity at T(liquid) [mPa*s]	Standard Error [mPa*s]	Slope [mPa*s/K]	Standard Error [mPa*s/K]
radial	3.6683	3.3639	−0.0273	0.0351
axial	8.0430	2.3993	0.0245	0.0239
merged	7.8422	2.0863	0.0148	0.0218

Zr3atOxPF2014BDay3Pb13

	Viscosity at T(liquid) [mPa*s]	Standard Error [mPa*s]	Slope [mPa*s/K]	Standard Error [mPa*s/K]
radial	3.3286	3.5400	−0.0302	0.0370
axial	6.9911	2.6549	0.0155	0.0266
merged	6.6237	2.2670	0.0046	0.0237

Abbildung 6: Zusammenfassung der Ergebnisse für die Zr3atO-Legierung.

3.5 Zr with 600ppm Oxygen

3.5.1 Comments on Datasets

According to the flight-log remarks there is only one experimental run without problems. That is parabola-flight 18. Data from Parabola-flight 16 looks also reasonable, although flight-log reports sticking problems at start.

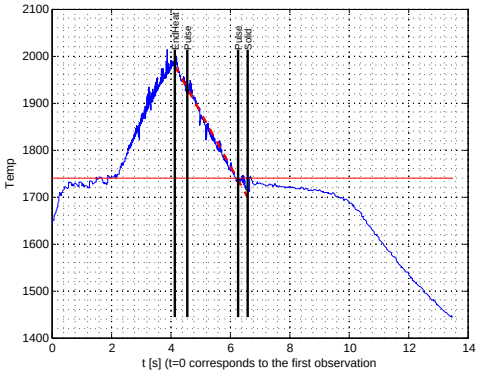

Abbildung 7: Zr600ppm0 Pb16

Pb 16

- Flight-log remark: Melt cycle, sticking problems at start.
- Edge-detection is sufficient. Sample-edges are regularly outside of camera-view. Therefore determined radii are corrupted.
- Second heat-pulse is $\approx 0.4s$ before resolidification.
- No supercooling (see Figure (7)).

Pb 17

- Flight-log remark: Contact to s.h. during heating.
- Temp and Heat-Power-Data are not in sync!
- Sample does not cool to Solidification-Temp. Dataset is not analysable.
- Sample rotates and oscillates remarkably wildly.

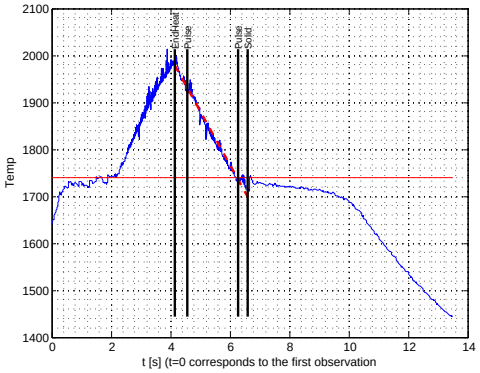

Abbildung 8: Zr600ppmO Pb18

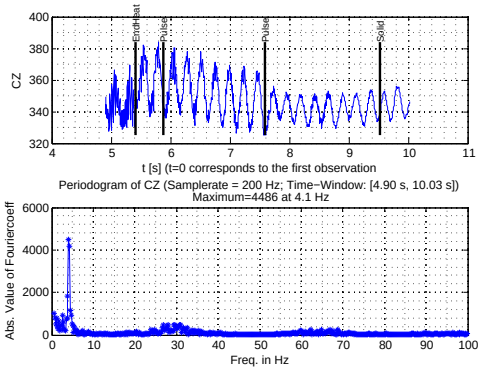

Abbildung 9: Zr600ppmO Pb18; Center of mass Coordinate CZ [pixel] vs time. Obviously the sample is systematically moving downwards.

Pb 18

- Flight-log remark: Melt cycle.
- Sample supercools approx. 120°C below Solidification-Temp. Latent Energy is clearly visible in Temp vs. Time Diagram (see Figure (8)).
- Primary Signals are of moderate quality. This might be due to the fact that the **sample edges are many times not in the view of the radial-cam** during the critical (liquid) phase of the sample.
- Sample moves systematically downward in the levitation field. (see Figure (9)).

Pb 19

- Flight-log remark: Contact to s.h. during heating.
- Dataset not analysable.

Pb 20

- Flight-log remark: Heater off at the beginning of the parabola.
- Sample does not reach melting-temperature. Dataset therefore not analysable.

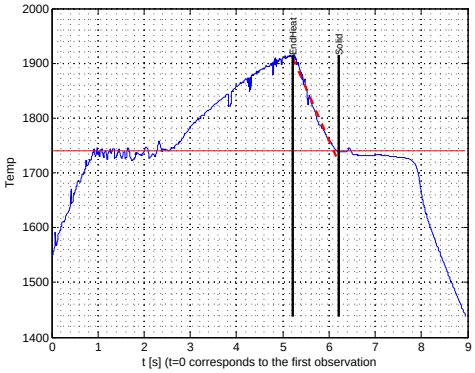

Abbildung 10: Zr600ppm0 Pb30

Pb 30

- Flight-log remark: Contact to s.h. during heating.
- Temp vs. Time diagramm looks very peculiar (see Figure (10)).
- No heat pulses during liquid phase of sample.
- Dataset is not analysable.

3.5.2 Results

4 Discussion/Remarks

4.1 Problems/Questions

- Timing of heat-pulses!?
- The primary signals (RX, RY, RZ, RXrot, RYrot and RZrot) are correlated, as well as the derived signals (e.g. sum, diff ...). It would be good practice to reduce the used signals on some almost independent signals. This decision has to be based on physical or experimental reasons.
- Are the variations of the signal-amplitudes really modulations or simply noise? One (obvious) problem that modifies the signal amplitude is when the **sample is not completly in the camera view. This occours regularly!**
- Oscillation/Movement of sphere in levitation-field can cause modulation of some of the observed variables, e.g. radii, sum of radii. This modulation should not occur in the difference of two radii. Question: Is this the main reason for the sometimes observed modulation? Rotation of the sample can also cause a modulation. *Superposition* of different modes can also cause a signal that looks like a modulation. Check Simulations and Sauerland [DisSa93].
  Experimental Facts to check:
  - Does modulation occur mainly/only in radius and sum of radii-variables, not in difference of radii.
  - Is the modulation-frequency the same frequency as the the center of mass oscillation.
  - Known Facts that support the hypothesis that oscillation of sample in eml-field is the main cause for modulation: Modulation-Frequency is always roughly 3 Hz. If sample-rotation is the cause for modulation, why should the sample always rotate with appproximatly 3 Hz?
  - What distance moves the sample during the experiments? How does this movement influence the signal (sample moves toward the camera implies bigger radii).
- BZ-Signal does not seem to be white-noise but has frequency peak at 30-40Hz and multiples! Why?

Literatur

[DisSa93] Stefan Sauerland, *Dissertation: Messung der Oberflächenspannung an levitierten flüssigen Metalltropfen*